university of groningen

faculty of science and engineering

UNIVERSITY OF GRONINGEN, GRONINGEN

MASTER RESEARCH PROJECT

Improving Fluorescence Detection and Heat Shielding for Cold Molecular Beam Sources

Student:
Thijs Qualm

Daily supervisor:
T. Fikkers
First examiner:
prof. dr. S. Hoekstra
Second examiner:
dr. A.O. Krushynska

June 2023

Abstract

To measure the electron Electric Dipole Moment (eEDM) more accurately the NL-eEDM collaboration aims to use a slow cold molecular beam of barium fluoride (BaF). Next to an existing source used for BaF, a new source is being designed. This source should be able to produce different molecules next to BaF, which could have more desirable properties to measure the eEDM. Part of this master project has been spent on improving the current BaF source by adding light shielding and setting up fluorescence imaging. With the experience gained from working with the current source, heat shields have been designed for the new source. These heat shields should allow the source to operate at low(er) temperature, be easy to maintain, and be modular in design.

Contents

1 Introduction

According to the Standard Model for elementary particle physics, the electric dipole moment of the electron (eEDM) is non-zero, but very small at most 10^{-38} $e \cdot$cm. [1] Various extensions of the Standard Model give larger values of the dipole moment, with some ranging from 10^{-27} to 10^{-30} $e \cdot$cm. [2, 3, 4, 5] Current eEDM measurment experiments cannot measure at the sensitivity required to verify the standard model's prediction, but they can verify or falsify various extensions. The upper bound on the eEDM is currently set at $|d_e| < 4.1 \times 10^{-30}$ $e \cdot$cm. [6] In this project light shielding has been built and fluorescence imaging has been setup, to improve an existing setup that aims to lower the upper bound on the eEDM using a cold molecular BaF beam. In addition to that, heat shields have been designed for a source for cold molecular beams that aims to be able to produce different molecules next to BaF, such as BaOH. This source will not replace the existing source but will be operated next to it. Operating and performing maintenance on the existing source helped me understand what should be changed when designing the heat shields.

The project to build the new source started around the same time as this project did and due to lead times on various components, the new source will not be operational within the duration of this project.

2 Context

2.1 Operation of the current source

A schematic of the current setup is shown in Figure 1. It consists of a cryogenic copper cell which is cooled down to 17 kelvin inside a vacuum chamber. A barium rod is placed inside the copper cell. Through a window inside the cell, an Nd:YAG pulsed laser is used to ablate some of the barium. SF6 gas is added via a tube and together with the just ablated Barium will create BaF. Neon buffer gas is added and via a small hole inside the cell a beam of molecules will form. The intensity of BaF molecules is measured by the absorption of laser light as it passes in front of the cell.

This beam of molecules will pass through a hexapole lens to focus it and part of it will be fed into a traveling-wave Stark decelerator. Here the beam forward velocity of the beam will be decelerated. A slower beam gives a longer interaction time during eEDM measurements, and therefore a more accurate measurement. During the project the traveling-wave Stark decelerator is out of order and the focus was on optimizing the BaF molecular beam. To get the most minimize the statistical uncertainty in eEDM measurements the beam needs to be as intense, cold, and slow as possible. In addition to this, the source needs to operate reliably for around 24 hours, preferably longer.[7]
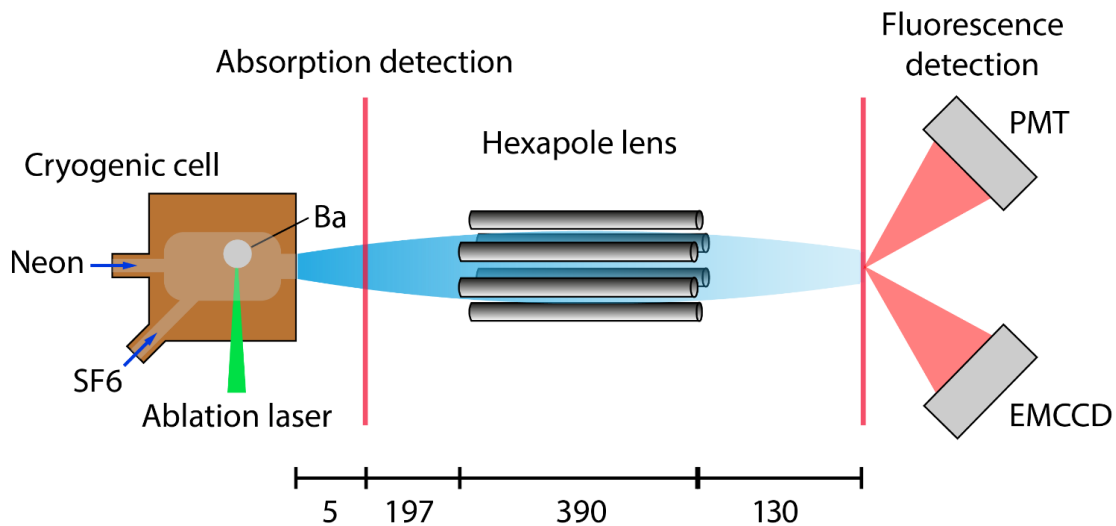
Figure 1: A schematic of the existing source which produces BaF, not to scale. The Neon and SF6 gas-flows are indicated by blue arrows. Inside the cryogenic cell a Nd:YAG pulsed laser (shown in green) ablates a barium target (shown in grey). The intensity of the molecular beam (shown in blue) coming out of the cell is probed by measuring the absorption of an intersecting laser beam (shown in red). A hexapole lens uses the Stark-effect to focus the molecular beam. The beam is measured using the fluorescence of the molecules hitting a laser beam (shown in red). This is done using a photo multiplier tube (PMT) and electron multiplying CCD camera (EMCCD). The scale at the bottom gives the distance in millimeters. The red lines at the absorption and fluorescence detection indicate laser bundles. Adapted from original made by J.W.F. van Hofslot.

To detect the BaF beam after it passes through the hexapole lens, a laser can be used to

excite the BaF molecules so that they will fluoresce. I will describe briefly how the fluorescence of BaF works. When light with the right frequency hits a molecule it can excite it from the ground state to an excited state. This excited state has a certain lifetime before it will decay, and when it decays it will emit a photon. The wavelength of this photon depends on the energy of the transition.

A simplified schematic of the relevant states in BaF is shown in Figure 2. The transition used for fluorescence is from the ground state $X^2\Sigma^+(\nu = 0)$ to the excited state $A^2\Pi_{1/2}(\nu = 0)$. From this excited state, the molecule has a 96 % change to fall back into to the same ground state, and emit a photon in a random direction. [8] The lifetime of this excited state is 59.6 ns [9]. The velocities in the beam are on the order of 200 m/s, meaning that the molecule will move on the order of 12 μm on average before emitting a photon. The molecules are excited with 860 nm laser light and the fluorescence is detected at 860 nm.
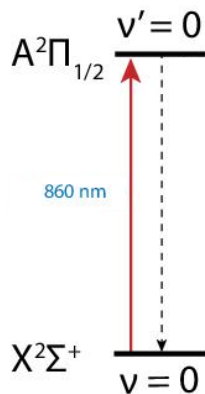

Figure 2: A schematic of relevant states for fluorescence measurements in BaF. Adapted from original made by J.W.F. van Hofslot.

For fluorescence detection, a Hamamatsu H7421-50 photo-multiplier tube (PMT) is used. This PMT can count separate photon pairs is bigger than 70ns, allowing for accurate measurements of time-of-flight data, as well as the total fluorescence count per shot. The downside of the PMT is that it only has a single pixel so it is not capable of creating spatial images.

To make spatial images an Andor iXon 897 Ultra electron-multiplying CCD camera (EMCCD) is used. This is a camera that uses electron multiplication to be more sensitive than a standard CCD camera. The molecular beam can be excited using a thin laser sheet. This light be captured using the EMCCD camera. This gives an image of the spread of the molecules for a cross-section of the molecular beam. A downside of the camera is the low temporal resolution. The camera has a maximum frame rate of 56 frames per second. [10] This means that a single frame takes 17 milliseconds. The spacing between the pulses of BaF is 100 ms, and at the fluorescence detection a single pulse is less than 10 milliseconds long. So unless the fluorescence laser is pulsed, the camera is not able to create any time-of-flight data.

For both of these measurements, it is desirable to have a high signal-to-noise ratio. A part of the noise comes from external light flooding into the vacuum chamber. A part of this project has been designing and manufacturing improved light shielding for these measurements.

3 Light shielding

3.1 3D Printing

During this project, a Prusa MK3s+ 3D printer was acquired. This is an FDM printer that will be used to print various materials such as PLA, PETG, and PC.

Because Prusa includes a magnetic height sensor (PINDA) in their print head, the printer can auto-level the printbed. This leaves the user with only one free variable, which is the offset between the PINDA sensor and the nozzle. This is set by the 'Live adjust Z' setting. We found that when changing the printing material the ideal value for 'Live adjust Z' also changes, This is something to keep in mind when changing the printing material. Up-to-date values for 'Live adjust Z' per material can be found on the printer frame.

3.2 Light Shielding

With the new 3D printer came many options to improve the setup. One of the problems that we had is that external light would be giving additional noise in fluorescence measurements using the PMT and EMCCD camera.

This was initially solved by using various blankets carefully wrapped around all the windows of the vacuum chamber. This worked well if all the blankets were in the right place, but it had two problems. If the blankets (partially) intersected the laser beam, for example when it exits the vacuum chamber, the blankets might scatter light back into the vacuum chamber causing increased noise. The second problem was that if the blankets left a small opening somewhere, external light could flood in and cause a high background. It was usually also hard to find the exact spot where the blankets left an opening.

Because we regularly changed the optics and camera position it was not possible to always leave the blankets in the same place. This meant that quite some time was spent on positioning the blankets correctly and measurements were done with sub-optimal noise levels.

The idea came that we could print custom light shielding that would exactly fit our setup, was easy to open, and easy to close. The vacuum chamber in which we measure the fluorescence is designed with laser cooling in mind and is referred to as the laser-cooling chamber. The laser-cooling chamber is cylindrical in shape and has four 160x40 mm windows at 90-degree spacing, and one CF150 window at the end. I will refer to the 160x40 mm windows as LCC windows. The laser-cooling chamber is shown in Figure 3.
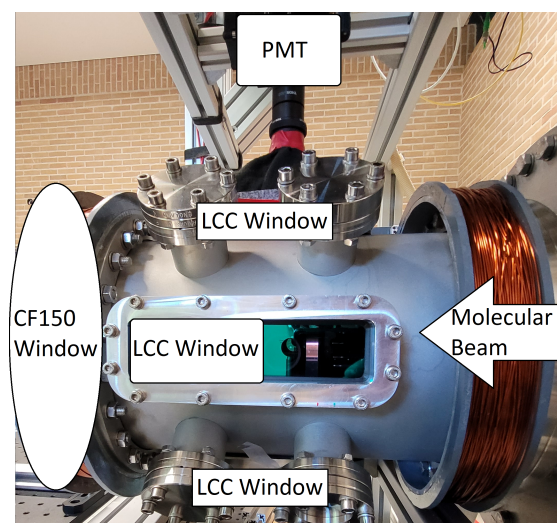
Figure 3: The laser-cooling chamber with 3 out of 4 LCC windows, a CF150 window, the PMT, and the molecular beam indicated.

In the next part, all printed light shielding is discussed. Because the shielding can consist of multiple parts which fit together, the choice was made to parameterize the designs. The parameters are stored in an Excel file so that they can be shared between multiple Inventor files. All final designs and Excel sheets are uploaded to the shared Evernote notebook, so they can be adjusted and reprinted if necessary.

Four main parts have been designed. A cover for the CF150 window, a basic cover for the LCC windows, a PMT-specific adapter for this cover, and a laser-safety-box adapter for this cover.

3.2.1   CF150 shielding

The CF150 window is currently not being used for any measurements, meaning the light shielding could be made quite simple. It is a lid that fits snugly around the window flange when a piece of cloth is glued to the inside. Currently, a piece of cardboard with black cloth facing the vacuum chamber is also underneath this lid.

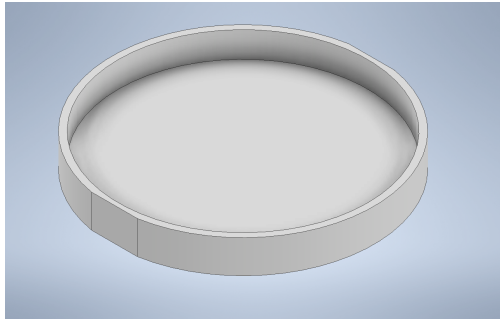Images of the design and the implementation are shown in Figure 4 and 5.

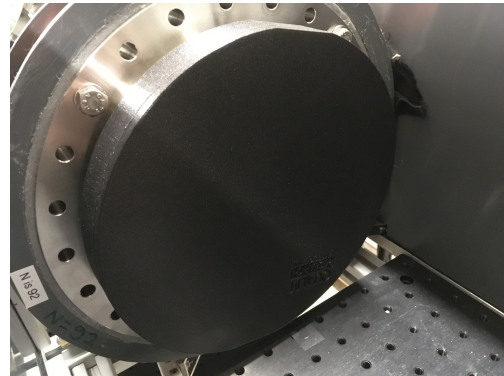Figure 4: The Inventor drawing of the CF150 light shielding.

Figure 5: The 3D-printed CF150 light shielding on the laser-cooling chamber.

3.2.2 LCC window shielding

The LCC windows were more challenging to design shielding for than the CF150 window, because they needs to be accessible for the camera, the PMT, and the fluorescence laser. Since the exact position at which the windows need to be accessed is subject to change it was chosen to make a sliding construction. Because I will be discussing this light shielding extensively I have decided to use the following terminology. The window is the 160x40 mm glass part through which light can enter and exit the vacuum chamber. The frame is the metal part surrounding the window. The rails are a 3D printed part that can be put on the frame. A cover is a 3D-printed part that can be slid into the rails and block light.

The idea is that every window would get identical rails, and for each window, specific covers could be printed. These covers could be smaller than the rails meaning it would be easier to print a replacement. For example to make a cover with a slit-shaped hole if the laser beam would be replaced by a laser sheet.

The initial design (V1) is shown in Figures 6 and 7. The rails are printed to exactly fit around the frame, with tight tolerances, so that it stays firmly in place due to friction. The cover is designed so that it slides easily, but is not loose.
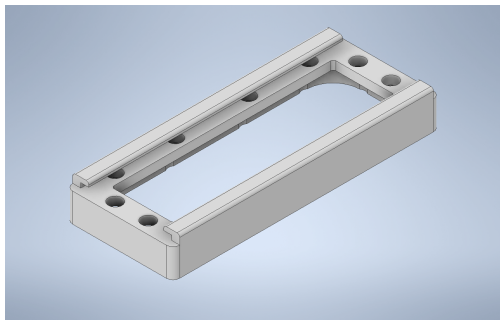

Figure 6: An Inventor drawing of V1 of the rails that is put on the LCC window.
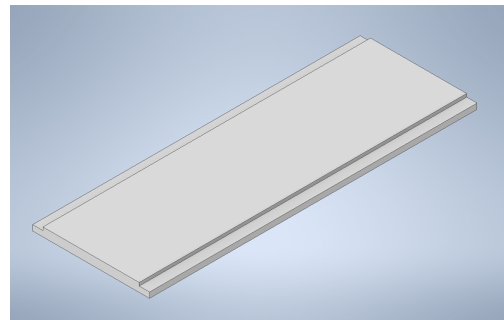

Figure 7: An Inventor drawing of V1 of the cover that can slide in front of the LCC window.

This design was printed and subsequently put on the vacuum chamber. Once it was installed

7

and tested, various adjustments and improvements were thought of. It was decided to make a new version of the light shielding which would not be compatible with this first version. This V1 rails and sliding cover is however still used on the bottom window because this window is currently unused and just needed to be closed off.

The following list of improvements was thought of and implemented in the second version of the light shielding (V2):

- Add a ruler on the outside of the rails. The ruler will consist of markings for 1, 5, 10, and 50 mm. The zero point is put in the center of the frame.

- The fit of the rails on the frame should be less tight. The rails will be easier to install and remove.

- Increase margins between the rails and covers, so the covers will slide easier.

- Bring the cover closer to the window, by reducing the thickness of the base of the rails. This reduces the space in the rails that was left for the bolts. The accessibility to the windows by the PMT and camera improves.

- Increase spacing between the two guides on the rails from 56.1 mm to 62.15 mm. The accessibility to the windows by the PMT and camera improves.

- Remove the fillet on the edge of the guides on the rails. Also, increase the thickness of the cover. These changes cause the top of the cover to be flush with the top of the guides. This makes designing covers that require a light-proof seal at the edges easier.

- Add a small lid to the end of the covers so that no light can leak in from the ends.

- Make an overlapping edge between two covers on the same rails. This way no light can leak between two covers.

- Add an indent in the covers in which cloth can be glued. Black cloth should do a good job at absorbing any stray light that hits it, and thereby reduce noise.

- Emboss sizes on the side of the rails. This way printed pieces can be recognized.

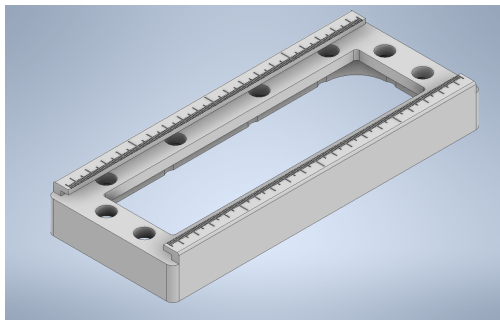In Figure 8 and 9 the updated cover and rails are shown.

Figure 8: An Inventor drawing of V2 of the rails that is put on the LCC windows.
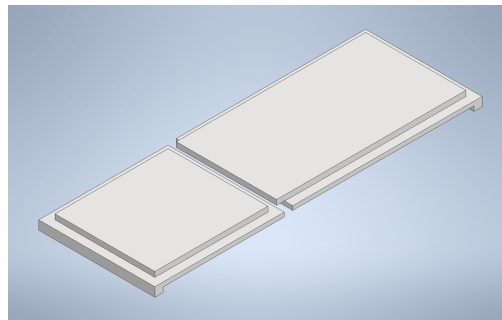

Figure 9: An Inventor drawing of V2 of the covers that can slide in front of the LCC window.

This version has been printed three times and is put on the remaining windows of the laser-cooling chamber. White Tipp-Ex is used on the ruler to make the markings easily readable.

3.2.3 LCC window PMT adapter

The PMT has a lens that is used to collect from the fluorescing molecules. The amount of light captures depends on the solid angle it covers. To maximize the solid angle, the lens is placed directly against the LCC window. A close-fitting cover has been designed to fit over this lens. This is shown in Figure 10. The design has been created as follows. A hole with the diameter of this lens was made inside the covers shown in Figure 9, at the position where both ends meet. To stop light from leaking through the edge of this hole a raised lid (the shape of two hollow half cylinders) was added. It was noticed that background counts from the PMT would also reduce if the entire lens itself was properly shielded against external light. So the cylinder was made to cover the height of the lens. The lens did however have an aperture that needed to stay accessible, so on one side the cover is not the full length of the lens. Since most of the background comes from external sunlight, the lamps in the lab do not seem to produce much 860 nm light, the tallest half cylinder should face the window. Some overlapping edges and lids were added to ensure there are no gaps through which light can leak into the laser-cooling chamber. The length of the covers is smaller than the length of the rails, but extra covers can be made to close off the edges of the window.
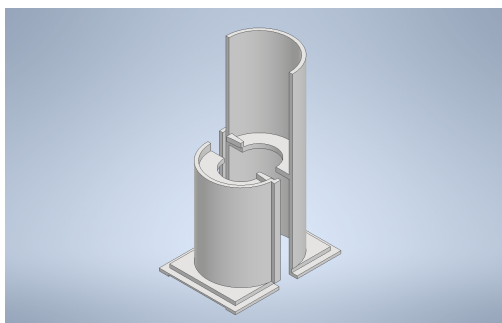

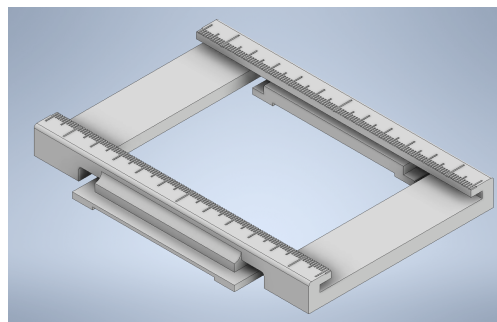Figure 10: An Inventor drawing of the PMT-specific cover for the LCC window.

Figure 11: An Inventor drawing of the perpendicular rails that allows for the second degree of freedom of the PMT position.

The exact location of the fluorescing molecules depends on the position of the molecular beam and the laser. Using a manipulator the PMT position can be changed to make sure it is pointing at the region of highest fluorescence intensity. With the light shielding installed, this should still be possible. Two options were considered. Designing a loose fit and using fabric close off the gaps. Or designing a tight fit that can slide. The loose fit was less preferable since it could give reproducible problems, with the exact position of the fabric being important.

It was decided to design a movable tight fit. The rails in which the light shielding is mounted already allow for 1 direction of movement. Adding a second layer of rails which would be perpendicular, would give two directions of movement. The final design is shown in Figure 11. This rails has the same dimensions as the one shown in Figure 8, so any cover can be fitted into it. It also has a ruler added so distances can be read easily.

The perpendicular rails was designed to have maximum accessibility of the LCC window, so the support beams are located on the outside of the rails. Fits are made as tight as possible to prevent any light from leaking through.

The final design mounted on the laser-cooling chamber with the PMT in place is shown in Figure 12.
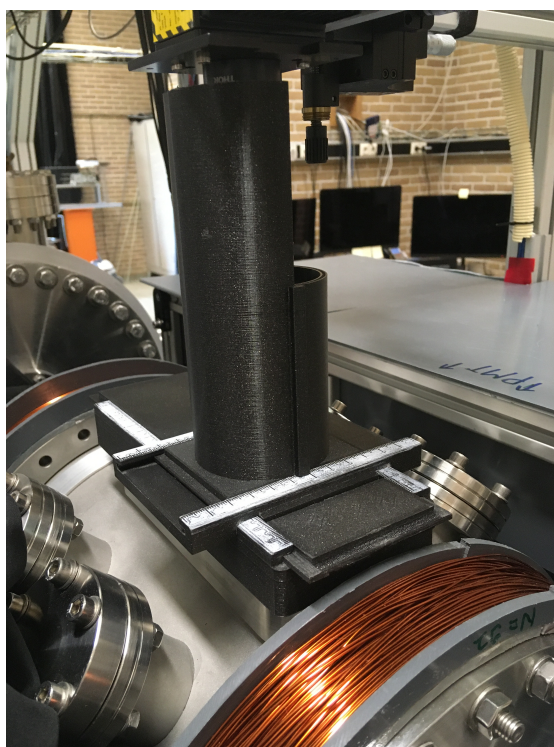
Figure 12: The light shielding of the LCC window through which the PMT measures fluorescence.

3.2.4   LCC window laser-safety-box adapter

At both sides of the laser-cooling chamber breadboard is placed on which optics are mounted to prepare the laser beam. Since the laser light used is class 3, it can be harmful to the eyes. To still create a safe environment a PVC box has been built around the optics on both sides of the laser-cooling chamber. This box also prevents external light from entering and creating noise in measurements.

There needs to be a cut-out in the laser-safety box around the LCC windows. This cut-out should not have gaps at the edges through which light could leak in, but this is difficult to achieve using just the PVC plate. So instead a separate adapter has been designed that makes sure there is an overlapping edge between the laser-safety box and 3D printed light shielding. It also is designed in such a way that it is easy to install and remove.

The design is shown in Figure 13 and consists of two parts. A schematic cross-section is shown in Figure 14. One part slides into the rails, this part is referred to as LSB frame in Figure 14. The second part fits onto the LSB frame, this part is referred to as the LSB rails in Figure 14. The LSB rails stays in place due to friction. The LSB rails has the same dimensions as the original rails, so all covers will fit.
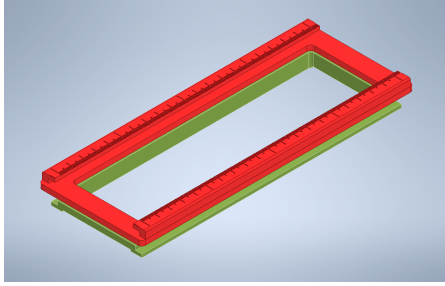
Figure 13: An Inventor drawing of the laser-safety-box adapter for the LCC windows.
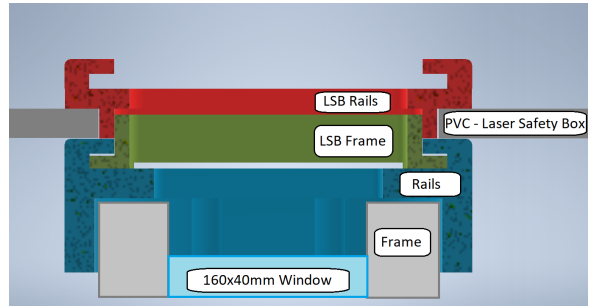
Figure 14: An schematic cross-section view of the installed laser-safety-box adapter for the LCC windows.

A photograph of the printed adapter is shown in Figure 15.
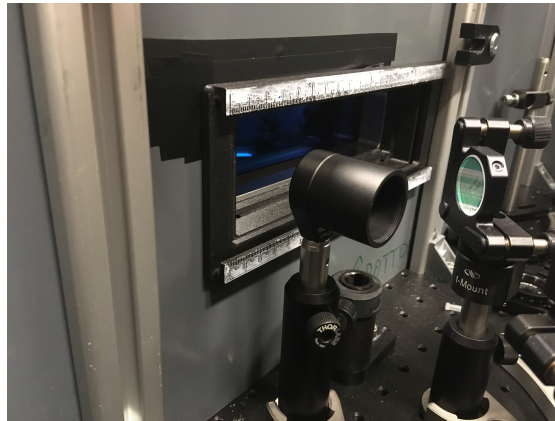
Figure 15: The printed laser-safety-box adapter installed on a LCC window.

3.3   Holder for neutral density filter

A small design was made for an adjustable holder for neutral-density filters. Neutral-density filters are used to control the power in our laser beams by absorbing a part of the light. The filters have a gradient such that on one side more light is absorbed than on the other. By changing the position of the filter, the power can be controlled.

Changing the position by moving the entire mount makes it hard to make small adjustments. The idea came to create a 3D-printed holder in which the neutral-density filter can be placed and easily moved. The final design is shown in Figure 16, and a printed and installed version in Figure 17. The design consists of a part that can be screwed onto a standard Thorlabs pole. This part contains rails with a hole for a set screw in which the second part can slide. The second part has a slot in which the neutral-density filter can be put and will be firmly held in place by friction.
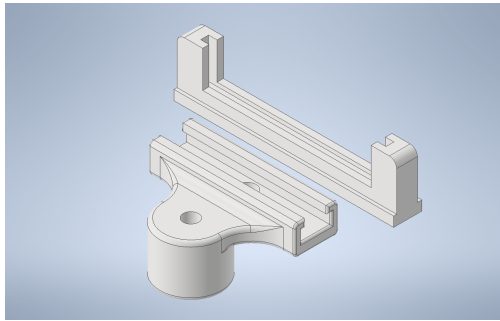
Figure 16: An Inventor drawing of the neutral-density filter mount.
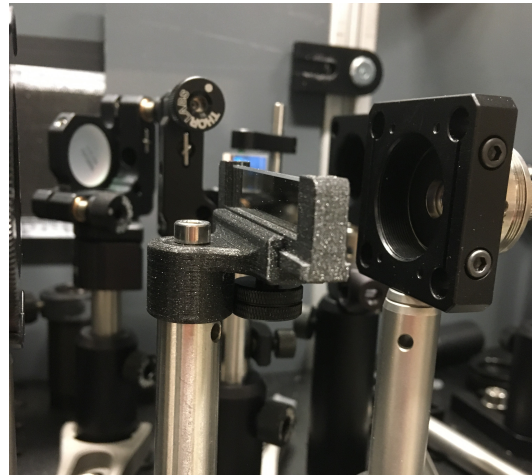
Figure 17: An photograph of the 3D printed neutral-density filter mount.

4 Imaging fluorescence

When optimizing the molecular beam for the eEDM experiment, it is useful to measure the distribution of BaF molecules in the beam. This can be done by using the fluorescence of the molecules. If a laser sheet is sent in perpendicular to the molecular beam the molecules will fluoresce at approximately the location where they hit the sheet, due to the relatively short lifetime (59.6 ns) of the excited state used for fluorescence.[9] This can then be imaged using a camera.

The camera used for imaging an Andor iXon Ultra 897 Electron Multiplying Charge Coupled Device (EMCCD).

4.1 Initial attempt at imaging

The initial setup included the camera at the end of the beam, looking into the vacuum chamber. A schematic of this is shown in Figure 18. This meant that the camera was looking perpendicular to the laser sheet.
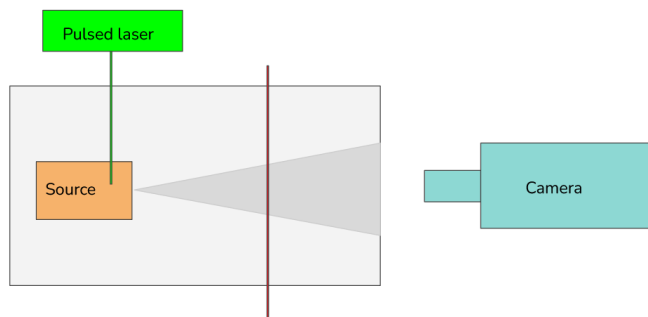
Figure 18: A simplified schematic top view of the setup used during the initial attempt at imaging. The vacuum chamber is indicated in light gray. The ablation laser is indicated in light green, the cryogenic cell in orange, the fluorescence laser sheet in red, and the camera in light blue.

The images produced by the camera however were overexposed. There seemed to be a step function in the image, where one side of the image was very bright and the other side empty. An example of this type of output is shown in Figure 19
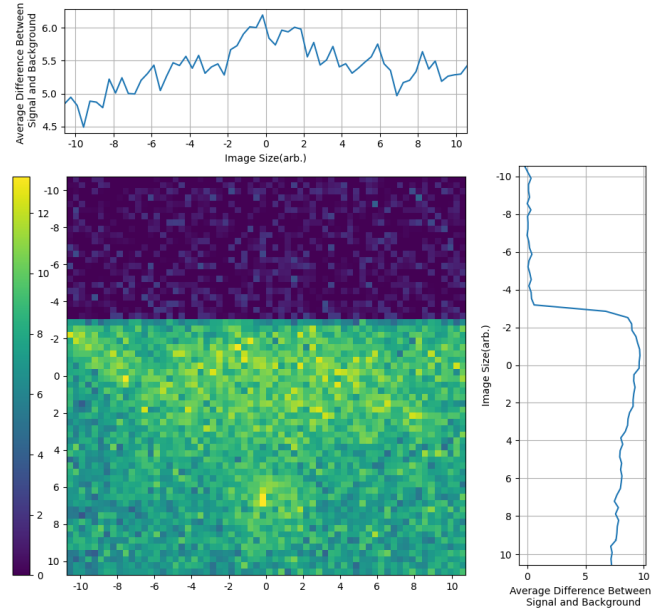
Figure 19: A net-signal image made with the camera looking perpendicular to the laser sheet. Intensity shows the signal image minus the background image. The size of the image and intensity have not been calibrated, so the units are arbitrary.

The light did not seem to come from fluorescence, since it appears both with and without the fluorescence laser on. It could also not be a background light since the background signal is recorded between pulses and removed from the signal.

We noticed that if we changed the time between the camera shutter opening and the ablation laser pulse the position of the step function would move. The shape of the step function suggested that it had something to do with the shutter or read out of the camera. To better understand this problem, the hardware manual of the camera was consulted.

4.1.1 Hardware details of Andor iXon Ultra 897

The information presented in this chapter comes from the hardware manual of the camera. [11] The internal structure of the camera is identical to a conventional CCD, but it has an additional multiplication register. This allows the camera to be less sensitive to the noise coming from the charge-to-voltage conversion, by increasing the charge before the conversion. This enhances the signal-to-noise ratio for this type of noise.

A schematic of the structure is shown in Figure 20. At the top part of the figure, the image section can be seen. This is the part of the sensor that is at the focal plane of the optics and in which charge builds up in the pixels. When an image has been captured by the pixels it can be moved down into the store section by using a vertical shift operation. Once the image is in the store section it will be moved down into the readout register line by line. For each line, the readout register will perform 512 horizontal shifts to read out all the pixels.

Figure 20: A schematic drawing of the pixels and registers inside the EMCCD which is to capture the images. Taken from [11].
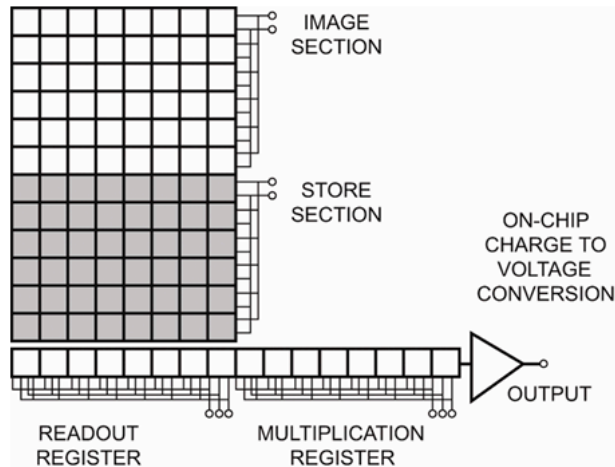
So far the image always is represented by a small charge inside a potential well (the pixels). To export the image it needs to be converted into a voltage and then it can be digitized. This happens using the on-chip charge-to-voltage conversion. This part is traditionally the biggest source of noise in a CCD camera, which is especially noticeable in low light conditions when the charge is very small. To counteract this an EMCCD camera has a multiplication register in which the charge is multiplied. The number of times an electron gets multiplied on average is called the gain. Electron multiplying is a probabilistic process in which every electron has a certain probability of exciting an additional electron when moving between potential wells. The probability of this happening is quite small for a single transfer (only 1 to 1.5 %) but over the length of the multiplication register, gains of up to a thousand times can be achieved.

The fact that the multiplication is random also introduces noise in the signal, which means that above a certain gain, the signal-to-noise ratio will not improve anymore. Because high gains cause the camera to age faster, the manufacturer recommends not using higher gains than necessary.

The camera does have a mechanical shutter to block incoming light, but this shutter is too slow to be used when taking images. The shutter has a maximum continuous operation speed of 2 Hz[11], while the ablation laser pulses at 10 Hz. Instead, the shutter is permanently open during measurements. This means that light is falling on the sensor and charge will build up. To move this charge away when the camera is not recording, the internal keep-clean cycle is activated. The keep-clean cycle consists of alternating vertical and horizontal shifts of the charge.

We operate the camera in an external trigger mode. We can use a BNC-connector to trigger the camera, where the high level has a minimum voltage of 2.2V, and low trigger has a maximum voltage of 0.88 V.[11] When the trigger is low the camera will continuously run the keep clean cycle. When the trigger becomes high it will stop the keep clean cycle, causing charge to built up on the sensor. Once the trigger becomes low again, the camera will move the image to the storage section, read it out, and send it via USB to the computer. During the read-out the keep-clean cycle is not active.

The external trigger is provided by the same trigger box used to trigger the ablation laser. If a bright flash of light hits the sensor, it will take some time before the keep clean cycle has

15

removed it. If during this time a recording is started a part of this bright flash will end up in the data, even if the flash occurred before the camera started recording.

4.1.2 Possible explanation for step function in initial images

In the initial images, we saw a step function in intensity. An explanation for this is that it is light coming from the ablation pulse, that is not yet cleaned of the sensor by the time the recording starts. In the image section the charge can only move in the vertical direction. If a recording starts while only half of the sensor is cleaned, the recorded image would show a step function, which would explain the initial images.

However, there are two reasons that it can't be light from the ablation laser itself. The first one is the wavelength, the ablation laser produces light at 532 nm. But the camera lens contains a Semrock FF01-860/11-25 860nm band-pass filter, which has an optical density of 7 at 532 nm.[12] A test was done where two of these filters were put in the lens, but the brightness of the step function had the same order of magnitude. This means that the light has to have a wavelength within the range where the optical density of the filter is at least less than 1, which is from 847 to 870 nm.[12]

The second reason is timing. The step function can still be seen 4.5 milliseconds after the ablation laser is triggered. The time it takes for the keep clean cycle to do 512 vertical shifts is about 0.5 milliseconds when using a vertical clock speed of 0.9 microseconds. This means the light should be emitted 4 milliseconds after the ablation laser is triggered, but the ablation laser pulse has a duration on the order of nanoseconds.

Taking this together, the theory was that an after glow of the ablation pulse is responsible for the step function. A way to get rid of this would be to remove the direct line of sight from the camera into the source. This was done by placing the camera at an angle of 60 degrees with respect to the LCC chamber. The camera is now looking through the LCC windows. A schematic of this setup is shown in Figure 21. This solved the issue and we were able to image the molecular beam.

Even though changing the line of sight solved the problem, there are problems with this theory. The steepness of the step function would indicate that the afterglow disappeared within less than 20 vertical shifts, meaning less than 10 μs. And because the images are averaged over 1000 shots it would have to always disappear within that time window. It seems unlikely that a after glow which stays for several milliseconds would end on such a small time window consistently. It might be possible that it was a problem in the camera settings which was (accidentally) solved at the same time the camera was moved. Further research has to be done to check if it might be possible to use the camera in the original configuration, with the current settings.
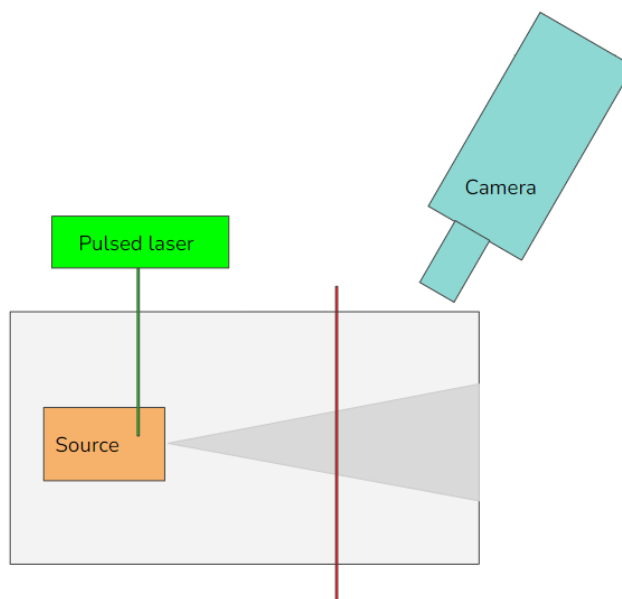
Figure 21: A simplified schematic top view of the setup used to successfully image fluorescence. The vacuum chamber is indicated in light gray. The ablation laser is indicated in light green, the cryogenic cell in orange, the fluorescence laser sheet in red, and the camera in light blue.

4.2 Designing the camera lens system

4.2.1 Requirements for the camera lens system

The requirements for the lens system are as follows. The focus should lie at the intersection of the molecules and the fluorescence laser. With the new position of the camera, this should be 18 cm from the first lens of the camera.

There is also a constraint on the length of the entire camera and lens system because the camera needs to fit inside the existing Boikon frame. This meant that the lens system itself should not be longer than 11 cm.

The lens should capture as much light as possible. To do this the solid angle is maximized by using the biggest lens available, which is a 2-inch f=90mm lens. All other lenses are 1 inch and available with various focal lengths.

Since we are looking at the laser sheet from under an angle we would like the depth of field to be big enough to make the entire image sharp. The molecular beam we want to image has a diameter of about 20 mm. We look at the image at an angle of about 60 degrees. If we make an approximation where the camera is infinitely far away compared to the image size we find that the depth of field we need is about 4 cm deep. The magnification and distance to the camera are set, so to increase the depth of field the aperture could be made smaller. This means less signal, so it should only be done if necessary.

4.2.2 Design for the Lens System

The lens system was designed as follows. First, an initial 2 lens system was designed using lens equations. Then, the lens design is made using ideal lenses in a ray tracing simulator. [13] The fluorescence was simulated as a point source, and the sensor as a 'line blocker'. The 2-inch lens

17

was placed in the known position at 18 cm from the light source. Various 1-inch lenses were put into place to see which set of lenses gives the right focus and fit within the length constraint. Using a ruler the magnification of the lens system was also estimated.

In this simulator, only ideal lenses are used. I found that using distances from this simulation to position lenses was too inaccurate and often the focus would not be good enough. So to set and check the focus without having to make images of molecules the following setup was used.

A torch with a piece of paper taped over the end, was placed to shine into the lens. On the piece of paper grid lines were drawn. The torch is positioned at the distance from the lens where the molecules would fluoresce. Then a projector screen is placed at the location of the sensor. For the Andor iXon 897 Ultra this is 17.4 mm behind the front plate of the camera. [11] When the lens system has the correct focus the grid lines should appear as an image on the cardboard. By moving the torch, the exact focus distance and depth of field were tested. Using this system a lens system was built which meets the requirements. Then this lens system is installed on the camera. The fluorescence of molecules hitting a small laser dot (200 μm beam waist) was used to fine-tune the focus by adjusting the position of the camera.

The final lens design starts with the 2-inch f=90mm lens, then 43 mm of space, followed by a 1-inch LA1509-B f=100mm lens, behind this lens a Semrock FF01-860/11-25 860nm bandpass filter is placed. The distance between the front plate of the camera and the 2-inch f=90mm lens is 88mm. The lens tube sticks out 12 mm in front of the 2-inch lens, making the entire system 10 cm long. The magnification has been estimated using the grid lines to be approximately 3. Using the height of the laser sheet the magnification has later been determined at 3.4. This makes the entire imaged area 27.5 mm tall.
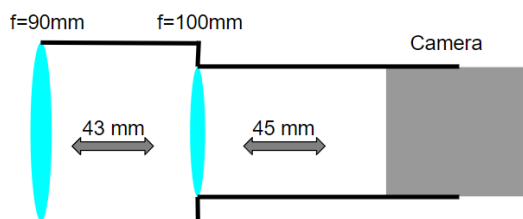
Figure 22: A schematic of the lens system. The f=90mm lens has a 2-inch diameter, the f=100mm lens has a 1 inch diameter. 43 mm indicates the distance between the center of both lenses. 45 mm indicates the distance between the center of the f=100mm lens and the front plate of the camera.

4.3 Creating a laser sheet

There are three requirements for the laser sheet. The first one is that it excites the molecules at a uniform rate at every height in the sheet. This means that the sheet should have a uniform laser intensity, or that it should have enough power so that it is well above saturation intensity. The second requirement is that it is as narrow as possible. If a sheet is not narrow it will result in blurry images, this effect is even more significant now that the camera is placed under an angle. The final requirement is that it is tall enough to capture the entire molecular beam. This means it should be around 20 mm tall. It is difficult to make it much taller because the mirrors used to send it into the laser cooling chamber have a 1-inch diameter.

4.3.1 Design of the Optics for a Narrow Sheet

The first attempt was to create a narrow laser sheet by taking a laser dot, expanding it using a beam expander. After a slit shaped aperture was used to create a laser sheet. This would make for an uniform if the diameter of the expanded laser bundle is significantly bigger than the slit. The problem with this method was due to diffraction the sheet will not stay narrow. Also, a significant part of the intensity is lost on the aperture.

A new design was made which solved these problems by using cylindrical lenses. The laser bundle, which has a Gaussian profile, is focused at the intersection with the molecular beam using spherical lenses. The beam waist for a Gaussian beam depends on the convergence, with a higher convergence giving a smaller waist. So to get a small waist, the laser light is first expanded using an LD1464-B f=-50mm bi-concave lens. The expanded beam is then focused using a LA1433-B f=150mm plano-convex lens. By changing the position of the LD1464-B lens the position of the focus can be shifted. A beam waist of about 350 micrometers is achieved like this.

If a smaller beam waist is desired the LA1433-B lens should be replaced by a lens with a smaller focal distance. The LD1464-B lens should then be replaced and re-positioned to get the focus at the correct distance.

To turn the spot into a sheet two cylindrical lenses are used. The first lens is an LK1836L1-B f=-9.69 mm plano-concave lens. This will expand the dot into a diverging sheet. An LJ1567L1-B f=100.00mm plano-convex lens is used to make the sheet parallel. A Gaussian beam cannot stay parallel, but because of the size of the sheet, it can be parallel enough for all practical purposes. If the size of the sheet is too small the LK1836L1-B can be moved closer to the LA1433-B lens. In this case, the LJ1567L1-B lens also has to be re-positioned.

4.3.2 How to align the optics for the laser sheet

I will describe how I aligned the optics. This does not have to be the best method and not the only method, but it might be useful for future readers.

- Start by aligning the laser dot from the fiber to go through the vacuum chamber and hit the molecular beam in the vertically in the center and at a right angle. The vertical center position can be found by optimizing the signal on the PMT. The angle of the beam can be optimized by making sure the laser hits the same location the LCC windows through which it enters and exits. The ruler on the 3D printer rails can be used for this.

- Install a Thor labs cage system for the two spherical lenses. Make sure that the cage system is at the exact center of the beam using apertures. Then install the system one lens at a time making sure that the lenses are centered by checking the position of the laser beam at a faraway distance.

- Once the cage is centered, the laser beam can be focused at the intersection of the molecular beam. This spot lies in the vacuum chamber, but by folding away the last mirror you can place a beam profiler at the equivalent distance. Using the beam profiler the beam diameter can be measured accurately.

- Install the cylindrical lenses one at a time, making sure that the center of the beam does not move. By changing the spacing between the cylindrical lenses the sheet can be made parallel.

- To ensure that the laser sheet has a symmetric intensity profile the beam profiler can be used. Make sure to turn off 'autoscale to peak' in Thorlabs Beam. Multiple beam-profiler measurements are needed to get a complete image of the laser sheet's intensity,

because of the height of the beam-profiler (9 mm) and the sheet (20 mm). If the sheet has an asymmetry in height, change the height of the first lens, then use the second lens to recenter the sheet vertically.

- The edges of the sheet can be cut off using an aperture. The edges are sometimes quite noisy and clipping of the last millimeter often gives a nicer intensity profile.

A final beam profiling measurement, at the equivalent position to the molecular beam, is shown in Figure 23. The beam profiler used is a Thorlabs BP209-VIS/M, and meant to profile Gaussian beams, so it is not optimal for measuring laser sheets. It can for example be seen that on a global scale, the intensity is the lowest at the top of the sheet in Figure 23. However, in every local measurement, the intensity is the lowest at the bottom. This sheet is relatively uniform but would require high laser power to ensure that the intensity is well above the saturation intensity and so that the variations do not matter.
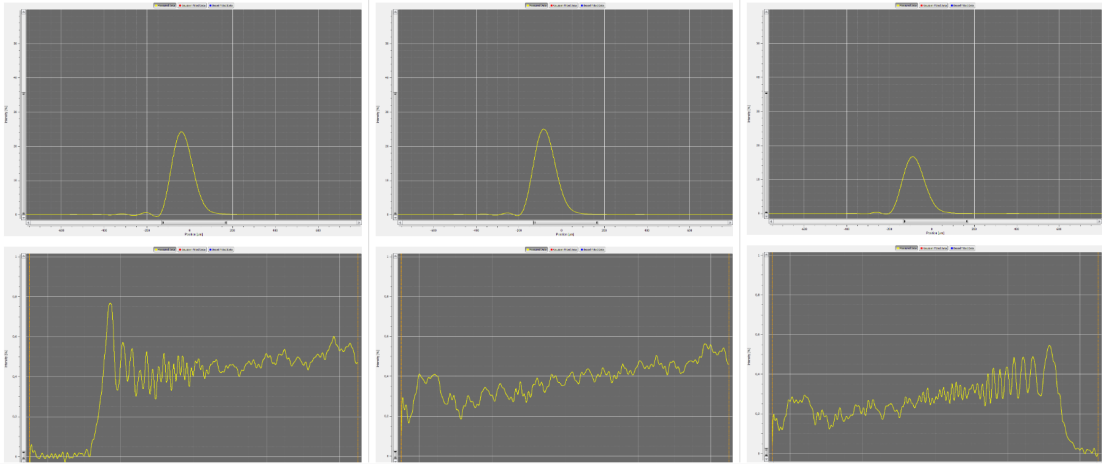

Figure 23: A profiling measurement of a thin sheet. The height at which the profiler was set from left to right is: 11.95 cm, 12.55 cm, and 13.40 cm. The sheet width from left to right is: 183 μm, 190 μm, and 191 μm. An indication of intensity values given as [left side plot, right side plot] from left to right is: [0.4%,0.5%], [0.3%,0.5%] and [0.2%,0.4%].

4.4 Upgrading maximum duration for camera images

When making images it is often useful to average over many shots, because the signal-to-noise ratio will improve with $\sqrt{N}$ where N is the number of images. The problem was that we were limited by the size of images we could make in one run. Every 2500 shots we would have to manually restart the camera in the software because of two reasons. The first reason was that the Python program that reads the files crashed unpredictably when the files got too big. Secondly, all the images should fit inside the working memory of the laptop on which they are recorded. I will discuss them here so that in the future this same problem will hopefully not be encountered.

4.4.1 Changing Python to 64-bit

The Python package reading the files will crash if the file size of a recording approaches 1 GB. The crash happens with the following error:
"OSError: [WinError 8] Not enough memory resources are available to process this command"

This means the program is running out of memory, seemed strange because the computer itself has plenty of memory available at this time. After some searching the cause turned out to be caused by the 32-bit Python version. This by default only has 2 GB of memory available. [14]

Because the computer on which the images are saved also runs important other Python programs for the experiment, such as 32-bit PicoScope, it was not desirable to replace the Python installation. Instead, a second version of Python is installed next to it. When using this 64-bit version of Python there are no problems anymore with reading in big files. When using this in for example Visual Studio keep in mind that you should open "Command Palette" search for "Python: Select Interpreter", and then select Python 3.10 (64-bit).

4.4.2 Spooling Images Directly to Disk

When trying to collect many images in one go using auto-save, the camera program will refuse when the file size was bigger than the working memory of the laptop. This was only 4 GB but was doubled to 8 GB when we changed the laptop. This is enough for measurements up to 20 minutes, but sometimes it is desirable to make longer measurements. It was pointed out to me by a former student that the camera is capable of directly writing the images to disk without keeping them in working memory. This function is called spooling and can be done by changing the settings of the camera program. With this in place, measurements lasting multiple hours or entire nights are now possible.

An example of an image averaged for 2695 shots (close to the initial limit) versus an image averaged for 30000 shots is shown in figures 24 and 25. It can be checked if the noise satisfies the $1/\sqrt{N}$ behavior. It should hold that $E_1/E_2 * \frac{\sqrt{N_1}}{\sqrt{N_2}} = 1$, where E_1 and E_2 are the noise in the first and second image respectively. N_1 and N_2 are the number of shots in each image. When we calculate this on the image below we find that $\frac{0.89}{0.27} * \frac{\sqrt{2695}}{\sqrt{30000}} = 0.99$ which is within the rounding error.
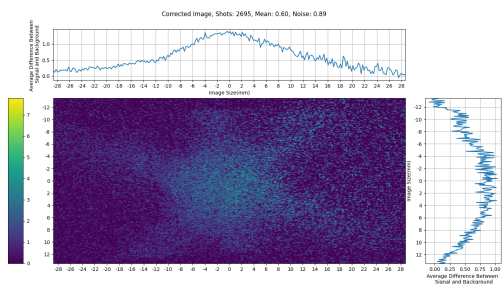

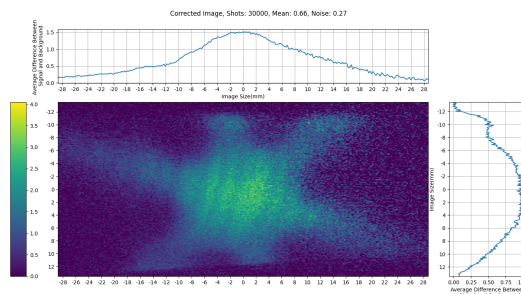Figure 24: A camera image of fluorescence, averaged over 2695 shots.

Figure 25: A camera image of fluorescence, averaged over 30000 shots.

5 Heat shields for the new source

5.1 Designing 4K and 40K Shielding

For the new source, a new set of heat shields will be designed. These will be mounted on the cryocooler and shield the cell against thermal radiation. The cryocooler used is an SHI RDE-418D4 two-stage Gifford-McMahon Cryocooler. This has two cooling stages, one stage which can provide 50 watt of cooling power at 50 Kelvin, and a second stage can provide 2 watt of cooling power at 4.2 Kelvin.[15] I will refer to the first stage as the 40K stage, and the second as the 4K stage.

In the current source the cell is mounted on the 4K stage and surrounding it are two heat shields. One mounted on the 4K stage and one on the 40K stage. The heat shields are there to block as much of the environmental black-body radiation as possible. From experience with the current source, it was noticed that often the limiting factor in the temperature at which we operate is the cooling power of the 4K stage. So we want to minimize the heat load at this stage.

To do this two heat shields are installed, one at each stage.

The function of the 40K shield is to protect the 4K stage from external radiation. And the function of the 4K shield is to freeze Neon and other gasses and to reduce temperature variations in the cell due to external radiative heat.

A rough calculation is done that will quantify the size of the heat load, and after this, the requirements are discussed. Finally, different iterations are used to explain the reasoning behind the final design. All the CAD models have been made in Inventor and are fully parameterized using an Excel sheet.

5.1.1 Estimations of heat load

According to the Stefan–Boltzmann law, the total intensity of black-body radiation per area is proportional to the temperature to the fourth power:

$$j^* = \sigma T^4$$

If we assume that the 40K stage is at approximately 40K and the environment at 290K we find that the ratio of incident power per area on the 40K stage to the 4K stage is:

$$\frac{j^*_{4K}}{j^*_{40K}} = \frac{40^4}{290^4} = 3.6 * 10^{-4} = 0.036\%$$

This means that the radiative heat load on the 40K stage will be much larger, than on the 4K stage if the 40K shield is perfectly closed. This is not a problem because the 40K stage has a much larger cooling power. A second implication is that the radiative heat load on the 4K stage will not come from the 40K stage, but from the holes inside the 40K stage. Because we need to send an ablation laser beam into the cell, an absorption laser beam in front of the cell and molecular beam out of the cell, there will be holes inside the heat shields.

If we assume that all radiative heat entering the 40K stage ends up on the 4K stage, we can calculate the heat load per unit square centimeter of hole in the 40K stage.

$$j^*_{290K} = \sigma T^4 = 5.67 * 10^{-8} * 290^4 \text{Wm}^{-2} = 401 \text{Wm}^{-2} = 0.04 W \text{cm}^{-2}$$

This means that about $50 cm^2$ of hole would correspond to all the available cooling power at 4.2K. The radiative heat load is not the only heat load on the 4K stage, so when designing the heat shields we should think of ways to minimize these holes.

It should be noted that the absorbed heat also depends on the emissivity of the shields. This is a number between 0 (perfect mirror) and 1 (black body) and depends on the wavelength, material, and surface finish. [16] The total absorbed radiation is an integration over all wavelengths, but to get an indicative value of the emissivity a single wavelength could be used. Using Wien's displacement law, The peak in black-body radiation at 290 Kelvin can be calculated to be 10 μm.

An inspection of surface emissivity at 10 μm wavelength for aluminum varies from 0.3 (oxidized) to 0.02 (unoxidized).[17] For copper the values can be higher, 0.2 to 0.9, when oxidized but can improve significantly when polished, down to 0.03. [16]

The outer dimensions of the 40K shield are 15 x 18 x 35 cm. When we assume an emissivity of 0.2 the total absorbed power from environmental radiation is about:

$$P_{Shield} = A j^*_{290K} \varepsilon = 22.8' \text{W}$$

Where A stands for the area, and P_{Shield} for the total absorbed power. This does not yet take into account the heat load on the part connecting the 40K shield to the 40K stage. The emitted radiation by the shield to the environment is negligible.

Ideally, we want the heat load on the 4K and 40K shields to be minimal, with as much of the heat load going to the 40K shield. This means the outside of the 40K shield should have a low emissivity, with minimal holes. The 4K shield and cell should also have low emissivity. If light ends up between the 4K and 40K shield it is more advantageous to be absorbed at the 40K shield, so the inside of the 40K shield should have high emissivity.

5.1.2 Requirements for 4K and 40K shields

The requirements of the 4K and 40K shields are mostly based on the experience we have with the current source. The following requirements were recognized:

- Since different molecules will be used, it is preferable that the cell is modular. It could be changed in length, and for example, charcoal sorbents could be placed to absorb helium.

- The source should be easy to maintain. Meaning that it should be easy to remove the shields and access the cell. Currently, some screws are hard to reach making it tedious to open the shields.

- Stripped screw thread should be avoided. Screw threads should preferably not be in copper, and if they are they should be long and in a part of the shield that is easy to replace. Buying a torque screwdriver for maintenance will also help.

- Areas in which holes are made should be easy to replace. This way no old unused holes are left in the 40K shield.

- It should be easy to manufacture. Using simple profiles, and/or flat plates will make it quick to build, and easy to make replacement parts.

- There should be enough space to allow for longer cells and added elements in front of the cell.

- The shields should be thick enough to transport all the heat efficiently. In the current source, the shields perform adequately, so this could be used as a reference. Ideally, the shields could be made slightly thicker since weight is not a restriction.

- There should be holes in the 4K shield for feed-through of at least two gas tubes, heating wires, and thermocouple wiring.

- The shields should have holes to let gas escape when pumping down from atmospheric pressure to the vacuum.

To simplify the design and production process the 4K and 40K shields, the same design will be used for both wherever possible. The designs are made fully parametric and linked to an Excel sheet, so the dimensions and thicknesses can easily be changed.

5.1.3 First iteration

For the first iteration, the focus was building a shield that was easy to build and maintain. The current source contained many screws making maintenance tedious. However the motor to rotate the target in the current source is not held in place by screws, but instead by metal clips which can be rotated into place. This makes it very easy to remove the motor. The idea was to make a rectangular box for both shields, from which you could remove the side panels with a clip-like system. The side panels would be attached to a frame. This frame could be made out of a simple profile and only needs to be cut to length, and cut at the ends to make the corners. The base plate would be more solid and milled out of a block. When designed like this the only difficult-to-replace part of the shield would be the base plate, but this would not contain any screws. The design is shown in Figure 26.
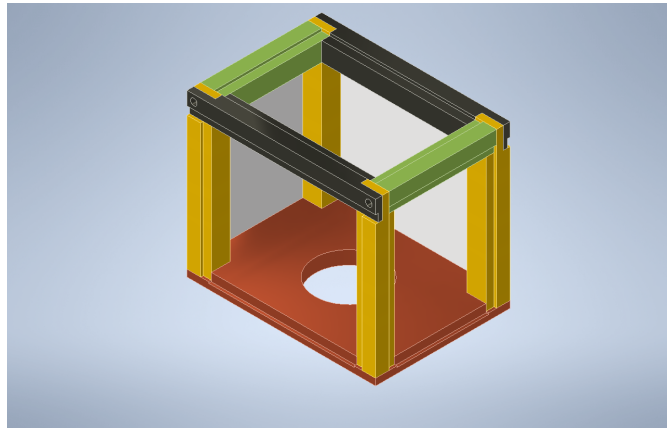

Figure 26: The first iteration of the design of the 40K shield drawn in Inventor. Colors are only for illustrative purposes, the entire shield is designed to be made out of aluminum. Three side panels have been removed for visibility. The dimensions are also arbitrary, with enlarged joints for illustrative purposes.

5.1.4 Final design

The design is simple to produce, but the corners are complicated and not very sturdy. This might mean that the cell can twist and have less than ideal thermal contact. So for the follow-up version, it was decided to combine the four top beams into one milled piece. The screws at the corner would be moved to the top, so all screw threads are in the easy-to-replace side poles.

For the 4K shield, additional changes were made. It was desired to have different sizes of 4K shields depending on which experiments are being done. Instead of changing the entire shield, it

was chosen to only shorten the side plates, and allow for a movable front plate. The baseplate and frame will still stick out if the cell is made shorter, but this should not be a problem. A breadboard pattern was made in the base plate which has multiple functions. It allows for easy mounting of the cell and a movable front plate. It also functions as a way to let gas out of the 4K shield when pumping from atmospheric pressure down to vacuum. It will also allow for the feedthrough of wires and tubing into the 4K shield.

The cell and the movable front plate position should be continuously adjustable. By using slots to bolt the cell to the 4K base plate this is achieved. To avoid the cell can move off-center or turn, a 1.5 mm deep slot is made in the base plate.
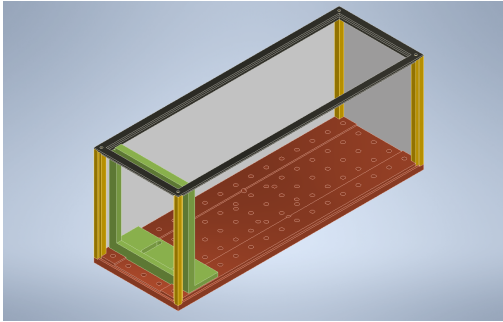
The final design in shown in figure 27 and 28.

Figure 27: An Inventor drawing of the 4K shield. Colors are chosen to highlight different components. The base plate is shown in red, the movable front shield in green, the pillars in yellow, the top plate in black, and the side panels in grey. Note that the side panels have been removed on three sides and from the movable front plate for illustration purposes. All components are made from copper.
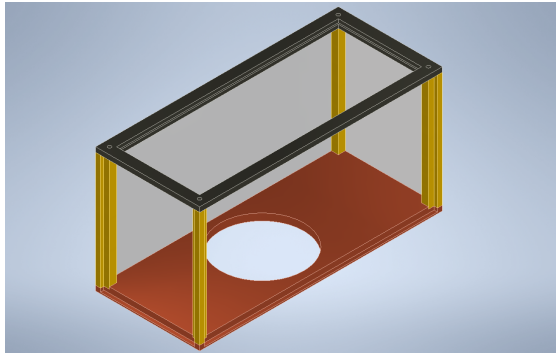

Figure 28: An Inventor drawing of the 4K shield. Colors are chosen to highlight different components. The base plate is shown in red, the pillars in yellow, the top plate in black, and the side panels in grey. Note that the side panels have been removed on three sides for illustration purposes. All components are made from aluminum.

6 Summary

This project set out with the intention of working on designing and building a new source suitable for creating slow molecular beams for eEDM measurements. During the project, the current source has also been improved by adding light shielding and setting up fluorescence imaging.

Light shielding has been designed and printed for fluorescence measurements. A standard rail system was designed that fits on all four rectangular windows of the laser-cooling chamber. Multiple covers have been designed that fit in the rail system. The light shielding is modular, easy to install, and still leaves the windows accessible without having to use tape or cloth to close holes. This means no time has to be spent anymore adjusting pieces of cloth to reduce the background.

A lens system and laser sheet for imaging fluorescence have been designed and built. A 20x0.3 mm laser sheet was used to excite molecules and using an Andor iXon 897 Ultra camera images have been made of fluorescence.

Heatshields have been designed that aim to allow the source to operate at low temperatures, as well as being easy to maintain and work with. Two shields have been designed, one for the 40K stage and one for the 4K stage on the cryocooler. Multiple iterations have been made and the final design consists of a base plate, on which four poles are screwed. On top of these four poles, a top plate is placed. The top plate has a rectangular hole to allow for maintenance without removing the top plate. During operation, 5 plates are used to close the four walls and the top plate.

For further research, it might be useful to look at the position and settings of the camera again. The explanation that was used to justify changing the position of the camera to get rid of a step-function in the images does not seem logical. It might be that the camera settings were the cause of this problem and that it was accidentally fixed at the same time the camera position was changed.

Due to the parametric design of the light shielding rails and covers, their dimensions can be changed easily. The same design could be re-used on the windows of the new source, or different windows of the existing source.

7 Acknowledgements

I would like to thank Ties Fikkers, my daily supervisor, for his valuable guidance and constructive feedback on the design of the heat shields and actively involving me in the development of the new source. I also thank Joost van Hofslot for familiarizing me with the source and its operation. Also, his insights and feedback on my thesis greatly contributed to its overall quality. I would like to express my appreciation to Anno Touwen for his assistance in setting up the camera and resolving technical issues. I am thankful to Leo Huisman for his expertise in designing the heat shields and for providing the necessary equipment. I wish to acknowledge the valuable input and suggestions provided by my second supervisor, dr. Anastasiia Krushynska, from the prospective of a different field of expertise. Finally, I am sincerely grateful to my first supervisor, prof. Steven Hoekstra, for his unwavering support, kind guidance, and valuable insights throughout my master's project.

References

[1] M. Pospelov and A. Ritz, "Electric dipole moments as probes of new physics," *Annals of Physics*, vol. 318, no. 1, pp. 119–169, jul 2005. [Online]. Available: https://doi.org/10.1016%2Fj.aop.2005.04.002

[2] Y. Nakai and M. Reece, "Electric dipole moments in natural supersymmetry," *Journal of High Energy Physics*, vol. 2017, no. 8, aug 2017. [Online]. Available: https://doi.org/10.1007%2Fjhep08%282017%29031

[3] S. M. Barr, "A Review of CP violation in atoms," *Int. J. Mod. Phys. A*, vol. 8, pp. 209–236, 1993.

[4] J. Engel, M. J. Ramsey-Musolf, and U. van Kolck, "Electric dipole moments of nucleons, nuclei, and atoms: The standard model and beyond," *Progress in Particle and Nuclear Physics*, vol. 71, pp. 21–74, jul 2013. [Online]. Available: https://doi.org/10.1016%2Fj.ppnp.2013.03.003

[5] W. Bernreuther and M. Suzuki, "The electric dipole moment of the electron," *Rev. Mod. Phys.*, vol. 63, pp. 313–340, Apr 1991. [Online]. Available: https://link.aps.org/doi/10.1103/RevModPhys.63.313

[6] T. S. Roussy, L. Caldwell, T. Wright, W. B. Cairncross, Y. Shagam, K. B. Ng, N. Schlossberger, S. Y. Park, A. Wang, J. Ye, and E. A. Cornell, "A new bound on the electron's electric dipole moment," 2022.

[7] P. Aggarwal, , H. L. Bethlem, A. Borschevsky, M. Denis, K. Esajas, P. A. B. Haase, Y. Hao, S. Hoekstra, K. Jungmann, T. B. Meijknecht, M. C. Mooij, R. G. E. Timmermans, W. Ubachs, L. Willmann, and A. Zapara, "Measuring the electric dipole moment of the electron in BaF," *The European Physical Journal D*, vol. 72, no. 11, nov 2018. [Online]. Available: https://doi.org/10.1140%2Fepjd%2Fe2018-90192-9

[8] Y. Hao, L. F. Pašteka, L. Visscher, P. Aggarwal, H. L. Bethlem, A. Boeschoten, A. Borschevsky, M. Denis, K. Esajas, S. Hoekstra, K. Jungmann, V. R. Marshall, T. B. Meijknecht, M. C. Mooij, R. G. E. Timmermans, A. Touwen, W. Ubachs, L. Willmann, Y. Yin, and A. Z. and, "High accuracy theoretical investigations of CaF, SrF, and BaF and implications for laser-cooling," *The Journal of Chemical Physics*, vol. 151, no. 3, p. 034302, jul 2019. [Online]. Available: https://doi.org/10.1063%2F1.5098540

[9] P. Aggarwal, V. R. Marshall, H. L. Bethlem, A. Boeschoten, A. Borschevsky, M. Denis, K. Esajas, Y. Hao, S. Hoekstra, K. Jungmann, T. B. Meijknecht, M. C. Mooij, R. G. E. Timmermans, A. Touwen, W. Ubachs, S. M. Vermeulen, L. Willmann, Y. Yin, and A. Z. and, "Lifetime measurements of the $a^2\pi_{1/2}$ and $a^2\pi_{3/2}$ states in BaF," *Physical Review A*, vol. 100, no. 5, nov 2019. [Online]. Available: https://doi.org/10.1103%2Fphysreva.100.052503

[10] Andor, "iXon Ultra 897 EMCCD," 2022. [Online]. Available: https://andor.oxinst.com/products/ixon-emccd-camera-series/ixon-ultra-897

[11] ——, "iXon Ultra 897 Hardware Guide," 2022. [Online]. Available: https://andor.oxinst.com/downloads/view/ixon-ultra-and-life-897-hardware-user-guide

[12] IDEX Health and Science, "860/11 nm brightline® single-band bandpass filter." [Online]. Available: https://www.idex-hs.com/store/product-detail/ff01_860_11_25

[13] Y.-T. Tu and W.-F. Sun, "Ray Optics Simulation," 2 2016. [Online]. Available: https://phydemo.app/ray-optics/

[14] Microsoft, "Memory limits for windows and windows server releases - win32 apps," Jun 2022. [Online]. Available: https://learn.microsoft.com/en-us/windows/win32/memory/memory-limits-for-windows-releases

[15] SHI Cryogenics Group, "Rde-418d4 4k cryocooler series," Feb 2023. [Online]. Available: https://www.shicryogenics.com/product/rde-418d4-4k-cryocooler-series/

[16] Fluke Process Instruments, "Emissivity - metals." [Online]. Available: https://www.flukeprocessinstruments.com/en-us/service-and-support/knowledge-center/infrared-technology/emissivity-metals

[17] Engineering ToolBox, "Aluminum - radiation heat emissivity," 2003. [Online]. Available: https://www.engineeringtoolbox.com/radiation-heat-emissivity-aluminum-d_433.html